Iterative Estimation of Antarctic Sea Ice Extent Using SeaWinds Data

Quinn P. Remund and David G. Long
Brigham Young University, MERS Laboratory
459 CB, Provo, UT 84602
801-378-4383, FAX: 801-378-6586
remundq@ee.byu.edu, long@ee.byu.edu

Abstract— Polar sea ice extent is an important input to global climate models and is considered to be a sensitive indicator of climate change. An algorithm has previously been developed for sea ice extent detection using data from the NASA scatterometer (NSCAT). This paper discusses the extension of that algorithm to data from SeaWinds on QuikSCAT. Due to differences in the two instruments, several modifications to the algorithm are needed for adaptation to SeaWinds data. Enhanced resolution, reconstructed SeaWinds imagery is generated using the scatterometer image reconstruction (SIR) algorithm. Images of the modified polarization ratio, h-pol σ^o, and the h- and v-pol σ^o estimate error standard deviations are used in the discrimination. An iterative maximum likelihood classifier is developed to segment sea ice and open ocean pixels. Residual classification errors are reduced through binary image processing techniques. The resulting ice extent estimates are highly correlated with the NASA Team algorithm 30% ice concentration edges derived from SSM/I data.

1. INTRODUCTION

Polar sea ice extent and the spatial distribution of sea ice are important features for several reasons. First, the extent of sea ice has long been considered an important component in global geophysical processes. For example, the insulating nature of sea ice impedes heat transfer from the relatively warm ocean and cool atmosphere. In addition, sea ice typically reflects a large amount of solar radiation back into space which modifies the levels of energy absorbed by the earth. Finally, sea ice extent is commonly held to be a sensitive indicator of long term global climate change [1].

This paper describes the development of an ice extent mapping algorithm using SeaWinds scatterometer data. In section 2, some brief background is given about the original NSCAT ice edge detection algorithm. Section 3, describes the SeaWinds data parameters and their levels of sensitivity to the presence of sea ice. A description of the algorithm is given in the following section. Finally, implementation results are given.

2. BACKGROUND

An automated sea ice extent mapping algorithm which adapts to the temporal changes of ice and ocean NSCAT signatures was developed in [2]. The method used the enhanced resolution reconstructed SIRF [3] imagery of the NSCAT observed σ^o polarization ratio normalized to 40° incidence (γ) as well as the v-pol incidence angle dependence of σ^o (B_v) as primary discrimination parameters.

The joint distribution of γ vs. B_v is bimodal. Ocean and ice pixels are contained in the two separate component distributions. The algorithm used linear and quadratic segmentation techniques to identify sea ice and open ocean pixels. Error reduction was performed using a secondary discrimination parameter, the σ^o estimate error standard deviation κ. This parameter is sensitive to temporal and azimuthal variations in σ^o. The final step in the algorithm consisted of some basic binary image processing to reduce residual noise effects. The resulting edge was found to have good correlation with the NASA Team 30% ice concentration edge. Unfortunately, NSCAT was only operational from August 1996 through June 1997 due to a spacecraft solar panel failure.

Extending the NSCAT algorithm to SeaWinds presents several difficulties due to inherent differences in the instruments. While both are Ku-band instruments, SeaWinds differs significantly from NSCAT. NSCAT was a fan beam scatterometer allowing the collection of measurements at multiple incidence angles and at both vv and hh polarizations. On the other hand, SeaWinds uses a scanning pencil beam configuration with separate fixed incidence angles for vv and hh polarization scans. Due to increased coverage, SeaWinds imagery of the polar regions can be produced from only one day of data rather than the six days required by NSCAT resulting in improved temporal resolution. Though the SeaWinds measurement geometry precludes the generation of the two primary NSCAT discrimination parameters, γ and B_v, modified parameters can be constructed that exhibit significant sensitivity to the presence of sea ice. These are described in the following section.

3. POLAR SEAWINDS DATA

Four primary SeaWinds SIRF images are reconstructed for each one day interval: vv-pol σ^o at 54° incidence (A_v^{54}), hh-pol σ^o at 46° incidence (A_h^{46}), and the vv- and hh-pol σ^o estimate error standard deviations (κ_v and κ_h). Sample images are shown in Figure 1. Since the SeaWinds instrument does not collect similarly polarized measurements at multiple incidence angles, images of B_v or B_h cannot be generated. In addition, different vv and hh polarization incidence angles prevent estimation of the polarization ratio.

The first parameter is the modified SeaWinds polarization ratio, γ_{sw}, which is defined as the difference (in dB) between A_v^{54} and A_h^{46}. The resulting metric contains a mixture of po-

0-7803-6359-0/00/$10.00 © 2000 IEEE

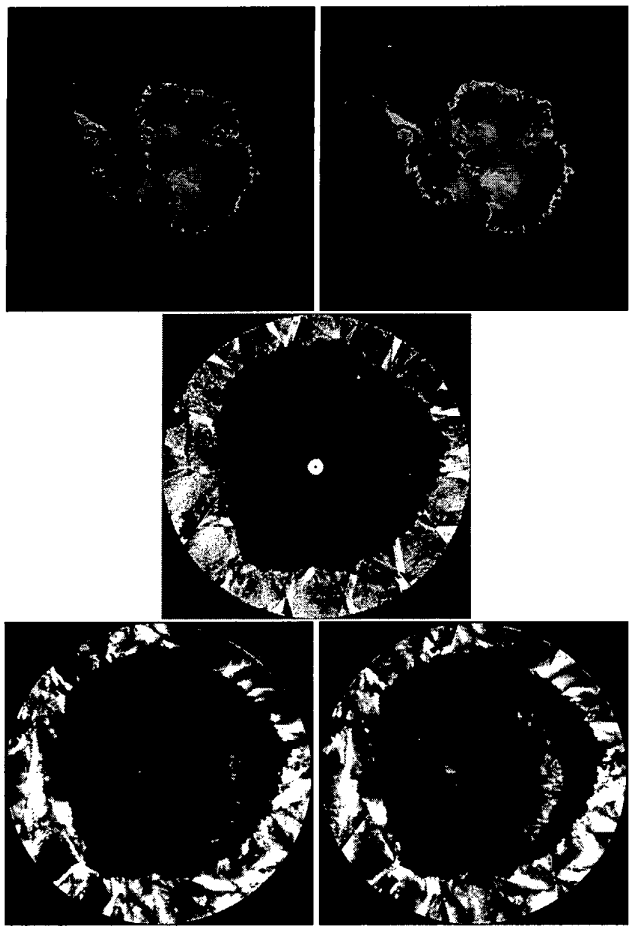

Figure 1: Sample SeaWinds SIR imagery for 1999 JD 240. The images are, from top left to bottom right, A_v^{54}, A_h^{46}, γ_{sw}, κ_v, and κ_h, respectively.

larization and incidence angle dependence. A sample image is shown in Figure 1. This figure illustrates that γ_{sw} values are, in general, high for ocean due to dominant surface scattering and low over the ice pack which is characterized by rough surface and volume scattering.

The A_h^{46} image is also useful in discriminating between ocean and sea ice pixels. A_h^{46} is typically much lower over the ocean than sea ice though wind induced ocean surface roughness introduces some ambiguities.

While the κ images were not useful as primary classification parameters for NSCAT data, κ_v and κ_h are in fact sensitive to the presence of sea ice. The longer imaging intervals required by NSCAT created greater dependence of κ on temporal variations which can cause ambiguous observations. In contrast, the SeaWinds images are created using only one day of data, reducing the effects of ice motion.

4. MULTIVARIATE SEA ICE EXTENT MAPPING

The four parameters (γ_{sw}, A_h^{46}, κ_v, and κ_h) form a 4-D hyperspace of measurement vectors that are used to identify the spatial distribution of ocean and sea ice. Production of 4-D histograms in this data space exhibit a similar bimodal nature as that observed in the NSCAT 2-D scenario. The first step in the algorithm performs a linear segmentation of the two modes by identifying the optimal hyperplane perpendicular to the line connecting the two distribution modes. The hyperplane is chosen such that it passes through the minimum histogram bin along the line. The linear segmentation results in an estimate of the location of sea ice and ocean pixels in the image.

While the linear method produces reasonable estimate of the ice edge, higher order classifiers can be used to improve the quality of the final sea ice map. A maximum likelihood (ML) classifier is derived assuming that the two component distributions are Gaussian in the hyperspace. Under this assumption, a maximum likelihood classifier reduces to,

$$C_{ML} = argmin_c \left[log|K_c| + (\vec{z} - \vec{\mu}_c)^T K_c^{-1} (\vec{z} - \vec{\mu}_c)\right] \quad (1)$$

where $\vec{z}$ is the feature vector, $\vec{\mu}_c$ is the mean vector, and K_c is the covariance matrix of ice type c. The ML method uses quadratic boundaries which account for the differences in component distribution variances and covariances. The required cluster mean vectors and covariance matrices are estimated from the linear discrimination result. These are used in the ML classifier to obtain another estimate of sea ice location. From this, $\vec{\mu}_c$ and K_c are updated and the ML scheme is used a final time.

The described technique is used for all pixels in the image except for pixels that were covered by less than four SeaWinds measurement footprints. In this case, the κ_v and κ_h parameters have too few observations to generate reliable estimates. As a result, these pixels are classified solely by an empirically derived threshold on γ_{sw}.

Though the ML images are reasonable estimates of the spatial distribution of sea ice, some residual errors exist. These are removed using basic binary image region growing techniques that eliminate small patches of ice erroneously identified as ocean and vice versa. While not common, additional large errors occur in regions that exhibited low wind speeds over the ocean for the imaging interval. As a result, the κ_v and κ_h values can be similar to lower ice values. The ambiguity causes the algorithm to fail in these regions. However, when they occur the regions are usually quite large and obvious. Many of these errors can be eliminated by constraining the observed ice edge advance and retreat. Through the use of binary image dilation and erosion procedures, the new ice edge estimate is compared with the previous estimate. If the edge has advanced or retreated beyond a specified threshold in a localized region, the previous day's edge is used in that region.

5. RESULTS

The algorithm was implemented for all daily images in the period 1999 JD 200-273 representing mid-July to the end of

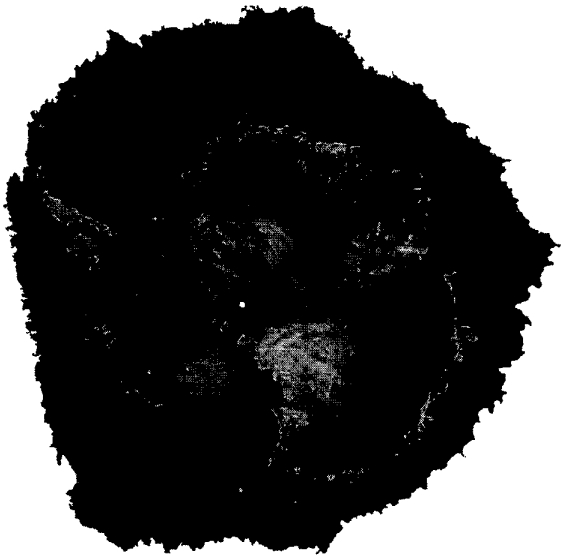

Figure 2: SeaWinds A_v^{54} image with ice mask applied for 1999 JD 240.

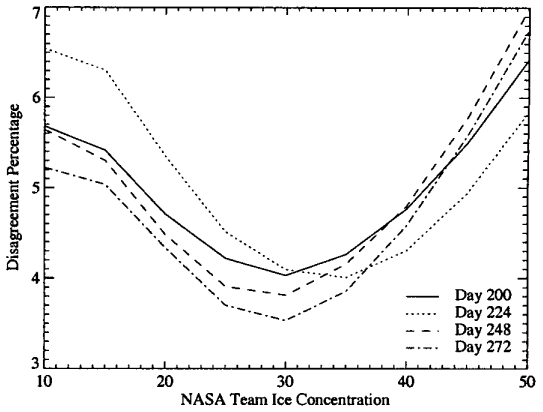

Figure 3: Disagreement percentage between SeaWinds and NASA Team ice edges as a function of ice concentration for four different days.

September. The algorithm appears to provide good estimates of the ice edge with only minimal obvious errors. A sample ice masked image is shown in Figure 2 for 1999 JD 240. We note that the algorithm identifies several narrow ice "fingers" protruding from the ice pack.

To provide a quantitative measure of the sea ice extent maps, the images are compared with NASA Team SSM/I-derived ice concentration images. The NASA Team algorithm uses polarization and gradient ratios computed from SSM/I data to estimate the ice concentration on a 25 km grid [4]. The ice edges at ice concentrations from 10% to 50% were compared with the SeaWinds ice edge at 5% increments. The disagreement percentage, ρ, is used to measure the dissimilarity between two ice edges. This metric is defined as the ratio of the surface area (in km) for which the two ice maps disagree to the area of the pixels classified as ice by either method. Hence high correlation in the edges should result in low disagreement percentages. Figure 3 shows the disagreement percentage between the SeaWinds and NASA Team edge as a function of ice concentration level for several representative days. In three of the four cases, the minimum is achieved at 30%. For the 74 daily images, 43 had minimum ρ at 30% concentration, 12 at 25%, and 19 at 35%. From these results, we conclude that the SeaWinds-derived ice edge is most similar to the NASA Team 30% ice concentration.

6. CONCLUSION

Previous studies have shown that Ku-band scatterometer data is capable of effectively discriminating between open ocean and sea ice. This paper demonstrated the development and implementation of a similar algorithm which uses SeaWinds scatterometer data. The technique is fully automated and adapts to temporally changing surface signatures. The resulting ice edges correlate best with the NASA Team 30% ice concentration edge. Though the algorithm was developed to map daily Antarctic sea ice extent, it can be applied to Arctic imagery.

7. ACKNOWLEDGMENTS

SeaWinds data was provided by the Jet Propulsion Laboratory. NASA Team ice concentration imagery was obtained courtesy of the National Snow and Ice Data Center.

REFERENCES

[1] W.F. Budd, "Antarctic sea ice variations from satellite sensing in relation to climate," *IEEE Trans. on Geosci. and Rem. Sens.*, vol. 15, pp. 417–426, 1975.

[2] Q. Remund and D. Long, "Sea-Ice Extent Mapping Using Ku-Band Scatterometer Data," *J. of Geophys. Res*, vol. 104, no. C4, pp. 11515-11527, 1999.

[3] D. Long, P. Hardin, and P. Whiting, "Resolution Enhancement of Spaceborne Scatterometer Data," *IEEE Trans. on Geosci. and Rem. Sens.*, vol. 31, pp. 700–715, 1993.

[4] Cavalieri, D.J., P. Gloersen, and W.J. Campbell, "Determination of sea ice parameters with the Nimbus-7 SMMR," *J. of Geophys. Res*, vol. 89, no. D4, pp. 5355-5369, 1984.